Final tau-neutrino results from the DONuT experiment

K. Kodama,[1] N. Ushida,[1] C. Andreopoulos,[2] N. Saoulidou,[2,*] G. Tzanakos,[2] P. Yager,[3] B. Baller,[4] D. Boehnlein,[4] W. Freeman,[4] B. Lundberg,[4] J. Morfin,[4] R. Rameika,[4] S. H. Chung,[5] J. S. Song,[5] C. S. Yoon,[5] P. Berghaus,[6] M. Kubantsev,[6] N. W. Reay,[6] R. Sidwell,[6] N. Stanton,[6] S. Yoshida,[6] S. Aoki,[7] T. Hara,[7] J. T. Rhee,[8] D. Ciampa,[9] C. Erickson,[9] M. Graham,[9] E. Maher,[9,+] K. Heller,[9] R. Rusack,[9] R. Schwienhorst,[9] J. Sielaff,[9] J. Trammell,[9] J. Wilcox,[9] T. Furukawa,[10] K. Hoshino,[10] H. Jiko,[10] M. Komatsu,[10] M. Nakamura,[10] T. Nakano,[10] K. Niwa,[10] N. Nonaka,[10] K. Okada,[10] B. D. Park,[10] O. Sato,[10] S. Takahashi,[10] V. Paolone,[11] C. Rosenfeld,[12] A. Kulik,[11,12] T. Kafka,[13] W. Oliver,[13] T. Patzak,[13,‡] and J. Schneps[13]

(DONuT Collaboration)

[1]*Aichi University of Education, Kariya 441-8522, Japan*
[2]*University of Athens, Athens 15771, Greece*
[3]*University of California/Davis, Davis, California 95616, USA*
[4]*Fermilab, Batavia, Illinois 60510, USA*
[5]*Gyeongsang University, Chiju, 660-701 Korea*
[6]*Kansas State University, Manhattan, Kansas 66506, USA*
[7]*Kobe University, Kobe 657-8501, Japan*
[8]*Kon-kuk University, Seoul, 143-701 Korea*
[9]*University of Minnesota, Minneapolis, Minnesota 55455, USA*
[10]*Nagoya University, Nagoya 464-8602, Japan*
[11]*University of Pittsburgh, Pittsburgh, Pennsylvania 15260, USA*
[12]*University of South Carolina, Columbia, South Carolina 29208, USA*
[13]*Tufts University, Medford, Massachusetts 02155, USA*

The DONuT experiment collected data in 1997 and published first results in 2000 based on four observed ν_τ charged-current (CC) interactions. The final analysis of the data collected in the experiment is presented in this paper, based on 3.6×10^{17} protons on target using the 800 GeV Tevatron beam at Fermilab. The number of observed ν_τ CC events is 9 with an estimated background of 1.5 events, from a total of 578 observed neutrino interactions. We calculate the ν_τ CC cross section as a function of one parameter. Assuming D_s mesons are the sole source for ν_τ, the energy-independent part of the total CC cross section can be parametrized as $\sigma^{\text{const}}(\nu_\tau) = 2.51 n^{1.52} \times 10^{-40}$ cm^2 GeV^{-1} for $n \geq 4$, where n is the parameter controlling the longitudinal part of the D_s differential cross section of the form $d\sigma/dx_F \propto (1 - |x_F|)^n$. The analysis could not distinguish between ν_τ and $\bar{\nu}_\tau$. The value of n obtained from PYTHIA simulations, $n = 6.1$, gives an estimated value of $\sigma^{\text{const}}(\nu_\tau) = (0.39 \pm 0.13 \pm 0.13) \times 10^{-38}$ cm^2 GeV^{-1}.

PACS numbers: 14.60.Lm, 02.50.Sk, 13.25.Ft, 13.35.Dx

I. INTRODUCTION

The tau neutrino, ν_τ, was assigned its place in the standard model after its electrically charged weak isospin-$\frac{1}{2}$ partner, the τ lepton, was discovered in 1975 [1]. The observation of identifiable ν_τ interactions, in a manner similar to ν_e [2] and ν_μ [3] interactions, did not immediately follow. The difficulty of measuring ν_τ interactions was due to the relative scarcity of the sources of ν_τ and the lack of sufficiently powerful detection methods to unambiguously identify the short-lived τ lepton (mean lifetime 2.9×10^{-13} s) produced in ν_τ charged-current interactions. These challenges were overcome in the ob-servation of four ν_τ interactions by the DONuT (direct observation of nu-tau) Collaboration, in 2000 [4,5], 25 years after the τ lepton was discovered. Analysis of our full data set yielded nearly 3 times as many neutrino interactions of all flavors as reported in Ref. [4]. This paper reports our final results, bringing the DONuT experiment to a completion.

The purpose of the DONuT experiment was to study ν_τ charged-current (CC) events,

$$\nu_\tau + \text{N} \rightarrow \tau^- + \text{X}, \quad \text{(1a)}$$
$$\bar{\nu}_\tau + \text{N} \rightarrow \tau^+ + \text{X}. \quad \text{(1b)}$$

However, during data taking, DONuT was recording inter-actions of neutrinos of all flavors: ν_e CC events,

$$\nu_e + \text{N} \rightarrow e^- + \text{X}, \quad \text{(2)}$$

ν_μ CC events,

---

*Present address: Fermilab.
+Present address: Massachusetts College of Liberal Arts, North Adams, MA 01247, USA.
‡Present address: Université Paris 7, Paris, France.

$$\nu_\mu + N \rightarrow \mu^- + X, \qquad (3)$$

and neutral-current (NC) events,

$$\nu_\ell + N \rightarrow \nu_\ell + X, \qquad \ell = e, \mu, \tau \qquad (4)$$

and analogously for the antineutrinos.

Reaction (1) must be distinguished from charm production in reactions (2) and (3), since the τ lepton and the charmed particles have comparable lifetimes and decay signatures:

$$\nu_\ell + N \rightarrow \ell^- + C^\pm + X, \qquad \ell = e, \mu \qquad (5)$$

where $C = D$, D_s, or Λ_c. Another background considered here was secondary hadron interactions in NC neutrino events, reaction (4),

$$\nu_\ell + N \rightarrow \nu_\ell + h^\pm + X, \qquad \ell = e, \mu, \tau, \qquad (6)$$

followed by

$$h^\pm + N \rightarrow (1 \quad \text{or} \quad 3 \, \text{prongs}) + X^0.$$

The production of two charm particles via NC neutrino interactions is a background process that is highly suppressed due to the mass of the created $c\bar{c}$ state and thus occurs at a rate too small to be of importance for this experiment.

The experimental apparatus and techniques have been described in detail elsewhere [6,7] and are only summarized here.

The location of vertices in the emulsion data, tagging leptons, and the subsequent search for secondary vertices were accomplished with high efficiency. This allowed a detailed event-by-event analysis with small and calculable background levels. Further, the large amount of information in the emulsion/spectrometer system permitted the use of powerful multivariate methods yielding probabilities for each candidate event to be signal or background.

The organization of this paper is as follows. First we give an overview of the neutrino beam and detector elements. Next, there is a synopsis of triggering and filtering that produced the interaction sample. We then give important details of the emulsion detector. The analysis is reviewed by outlining the lepton identification procedures,

Monte Carlo techniques, event location in the emulsion and secondary-vertex search. After a survey of the entire data set including neutrino interactions of all flavors, the ν_τ cross section analysis is described, systematic error sources are discussed, and the results are presented.

II. NEUTRINO BEAM AND DETECTOR

DONuT beamline.—The 800-GeV protons from the Tevatron were stopped in a beam dump in the form of a solid block of tungsten alloy having a cross section of 10×10 cm^2 and a length of 1 m. The typical intensity was 8×10^{12} protons for 20 s each minute, or about 20 kW of beam power. Immediately following the beam dump were two dipole magnets with solid steel poles, providing both absorption of interaction products and deflection of high-energy muons away from the beam center. Following the magnets was an additional 18 m of passive steel shielding limited to within 2 m of the beam line. Emerging at the end of this shield, 36 m from the beam dump, were neutrinos and muons. The muons were mostly contained in horizontal fanlike distributions on each side of the centerline. The neutrino beam design is shown in Fig. 1.

Primary beam.—The number of 800-GeV protons that struck the beam dump was measured by devices that integrate charge collected from secondary emission from a foil. These monitors were calibrated with a beta source before the experiment began. Several times during the course of the run, these devices were calibrated against coil pickups and other monitors installed in the accelerator extraction complex. These checks showed that the primary beam monitors were consistent within 5% at intensities of 5×10^{12} to 1×10^{13} protons per spill. Losses in the beam line were small ($\approx 10^{-5}$), and no other corrections were applied. The monitors' output was digitized and recorded at the experiment, and gated by the trigger electronics. A total of 3.54×10^{17} protons were recorded during the live time of the experiment. A systematic uncertainty of 5% was assigned to the value of the total number of protons in the beam dump.

Neutrino beam.—Neutrinos in the DONuT beam originated from decays of particles within the hadron shower
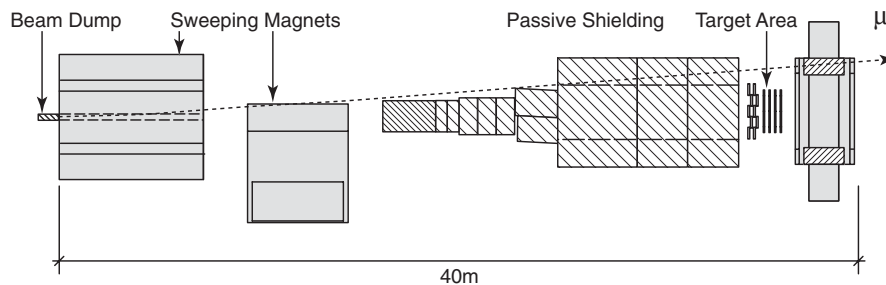

FIG. 1. Schematic plan view of the neutrino beam. The 800 GeV protons are incident on the beam dump from the left. The emulsion modules are located within the target area, 36 m from the beam dump. The trajectory of a 400 GeV/c negative muon is shown. Note that the passive steel shield does not fill the volume occupied by high-energy muons along the plane of the beam line.
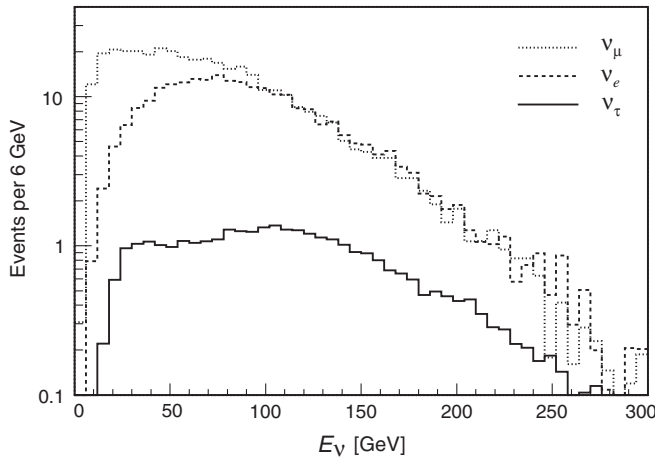
FIG. 2. Calculated energy spectra of neutrinos interacting in the DONuT emulsion target. The spectra were computed with values of n [Eq. (7)] derived from PYTHIA output.
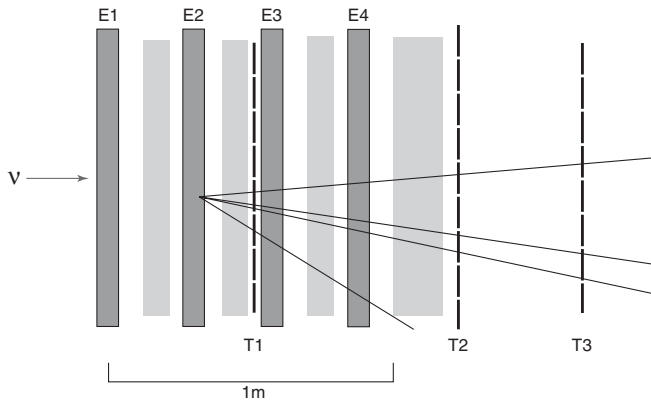

FIG. 3. Schematic plan view of the target region. The emulsion modules are indicated with E labels, the trigger hodoscopes with T labels. The lighter gray areas are occupied by scintillating fiber planes, 44 in total. The paths of charged particles in a typical interaction are superimposed.

created by a primary proton interaction. Neutrinos from decays of charmed particles are called *prompt* neutrinos, and neutrinos from decays of $\pi^{\pm}$ and $K^{\pm}$ are called *nonprompt* neutrinos. About 97% of the neutrino flux from the beam dump was composed of ν_e and ν_μ, the rest being ν_τ. 93% of the ν_e's were prompt, while ν_μ's had substantial components of both prompt and nonprompt neutrinos. All ν_τ's were prompt and at least 95% of them originated in leptonic decays of D_s mesons. The decay $D_s \rightarrow \nu_\tau \tau$, with the subsequent τ decay, yielded two ν_τ's within a distance of a few millimeters. Very few ν_τ's are lost from absorption of their parent particle in the beam dump since the interaction length (6 cm) of the parent is 30 times the mean of the decay lengths. The calculated neutrino energy spectra of all the neutrinos that interacted in the DONuT target are shown in Fig. 2.

Emulsion target.—The target—schematically depicted in Fig. 3—was the core of DONuT. Its capabilities and performance were matched to the task of recognizing neutrino interactions containing τ leptons. The main component of the target assembly was 260 kg of nuclear emulsion stacked in modular fashion along the beam line. A total of seven emulsion modules in the target station were exposed, with a maximum of four modules in place at any time during the experiment.

Each module was exposed for a limited time to avoid track density higher than 10^5 tracks per cm^2 that would make the emulsion data analysis inefficient. To further assist the analysis, single changeable sheets (CS) were mounted 1 cm downstream of each emulsion-target module and replaced 10 times more often.

Scintillating fiber tracker (SFT).—Integrated into the emulsion-target station were 44 planes of the SFT built using 0.5-mm-diam scintillating fibers to provide medium-resolution tracking and a time stamp for each event.

Spectrometer.—The emulsion-target station was followed by a spectrometer consisting of a large-aperture
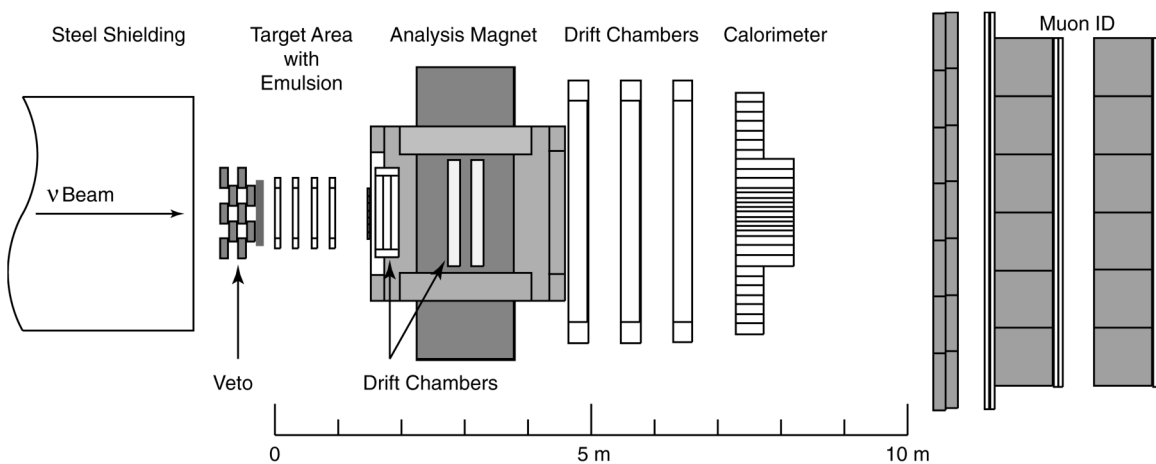

FIG. 4. Schematic plan view of the spectrometer. The neutrinos are incident from the left, emerging from the passive shield. The design is relatively compact to optimize identification of electrons and muons.

dipole magnet and six drift chambers. A lead- and scintillating-glass electromagnetic calorimeter aided in identifying electrons and measuring their energy. Behind the calorimeter, muons were tagged with a muon-ID system consisting of three steel walls each followed by two crossed proportional-tube planes. The plan of the spectrometer is shown in Fig. 4.

III. SPECTROMETER DATA COLLECTION AND REDUCTION

A. Triggering and data acquisition

Trigger.—A trigger for recording neutrino interactions required that no charged particles entered the emulsion from upstream and at least one charged particle emerged from an emulsion target. The scintillation-counter triggering system included a veto wall upstream of the emulsion target and three hodoscope planes distributed between and downstream of the emulsion modules, shown in Fig. 3. Although the average trigger rate was 5.0 Hz, the live time was only 0.89 due to the 30 ms readout time of the SFT system. The trigger efficiency was calculated using simulated neutrino interactions and measured efficiencies for all counters. The efficiency for triggering on ν_e CC, ν_μ CC, ν_τ CC, and NC interactions was 0.98, 0.96, 0.96, and 0.86, respectively. A detailed description of the triggering system can be found in Ref. [7].

Data acquisition.—The architecture of the data acquisition was based on the Fermilab DART product [8], using VME-based microprocessors to control the transport of data from the VME buffers to a host computer. The host computer served as both the data monitor and as the data logger to tape (Exabyte 3500). The average event size was 100 kB, with a throughput of 10 MB per beam cycle of 1 min.

B. Filtering and scanning

A total of 6.6×10^6 triggers from 3.54×10^{17} protons on target were recorded. In this data set, only about 10^3 neutrino interactions were expected. This implied that the great majority of the triggers were background processes satisfying the simple trigger requirements of Sect. III A. Data from the electronic detectors were used to extract the neutrino-interaction candidates in a two-step process.

Software filter.—The time difference between any two trigger counter signals was required to be within 2.5 ns. Data from the SFT and from the drift chambers were then used to reconstruct tracks and to search for a vertex near one of the emulsion targets. Triggers that did not yield a candidate vertex were eliminated. This software filter reduced the number of recorded triggers by a factor of 300. Efficiencies for keeping neutrino interactions were determined by Monte Carlo studies to be 0.98 (for CC events) and 0.96 (for NC events).

Physicist scan.—In the second step, the remaining triggers were scanned individually by two teams of physicists using a graphical display. Each of the two team members scanned all the events in one-half of the data. This step rejected events originating from particle showers produced by high-energy muons and checked for errors in reconstruction and other pathologies. Most of the events were rejected quickly and with high confidence. This visual scanning reduced the data by another factor of 20, yielding 866 neutrino-interaction candidates within one of the emulsion modules which had a visible energy over 2 GeV. The efficiency of the physicist scan was found to be (0.86 ± 0.07), as determined by each team rescanning 10% of the other team's event set.

The estimated total efficiency for retaining a ν_τ CC interaction with the electronic detectors was 0.72 after triggering, filtering, and scanning. For ν_e (ν_μ) CC interactions the total efficiency was 0.73 (0.71), and for NC interactions it was 0.64.

C. Neutrino event sample

The resulting sample included 866 events that were likely neutrino interactions of all flavors with the vertex located within the volume in the emulsion target.

We report here on the analysis of all the events for which the neutrino-interaction vertex was found in the emulsion, referred to throughout as "located events." Vertex location was attempted for 866 events, yielding 578 located events as described in Sec. VII. Events in the initial sample that were not located in the emulsion were discarded for the analysis described below.

IV. THE EMULSION

The DONuT emulsion modules were the first modern implementation of a design that interleaves metallic sheets (stainless steel) with emulsion sheets to increase the mass while maintaining the high precision necessary for τ recognition. As illustrated in Fig. 5, two designs of these "emulsion cloud chambers" (ECC) were used in DONuT: both used 1 mm thick steel sheets interleaved with emulsion sheets having 100 μm thick emulsion layers on both sides of a plastic base. The designs differed in thickness of the base: one was 200 μm and the other 800 μm thick. The third design had 350 μm thick emulsion layers on a 90 μm thick base. More details about the emulsion-target design can be found in Ref. [6].

After exposure, the emulsion-target modules were transported to Nagoya University in Japan, where they were disassembled and individual emulsion sheets developed. The CS were developed at Fermilab.

The information from a small emulsion volume surrounding the interaction point predicted by the spectrometer data was fully digitized and used in a manner similar to the information from an electronic detector. The size of the volume needed to be large enough to contain the vertex but small enough to be compatible with the capabilities of the emulsion scanning machines.
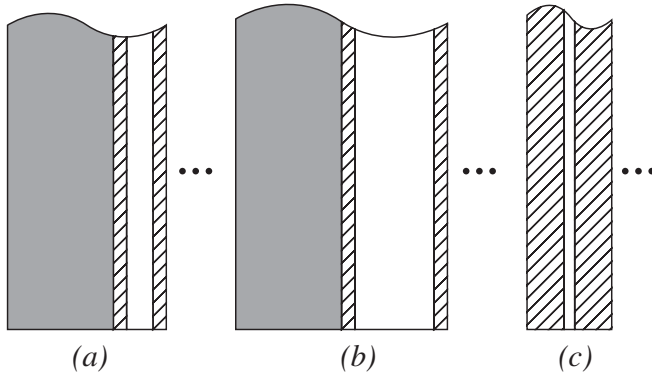
FIG. 5.   Emulsion-target designs. The ECC designs (a) and (b) used 1-mm thick stainless steel sheets interleaved with emulsion plates using 100-μm thick emulsion layers on a 200-μm plastic base in (a), and 800-μm plastic base in (b). Most neutrino interactions were in the steel. The bulk emulsion type (c) used 350-μm emulsion layers on a 90-μm plastic base, without steel. Steel is indicated by shading, emulsion by crosshatching, and the plastic base is unshaded.

Once the desired emulsion volume was determined, the individual emulsion sheets were digitized using an automatic scanning and digitizing apparatus at Nagoya University. The Nagoya group developed this technology over the years, starting in 1974. The DONuT emulsion data were obtained using ultratrack selector (UTS) digitizers [9]. With this system, the emulsion sheets were scanned and digitized at a rate of 1 cm^2 per hour, a factor of 5 improvement over the technology used to obtain the first DONuT results of Ref. [4], allowing for greatly increased location efficiency.

Emulsion data.—The UTS automated scanning stations found and digitized track segments (''microtracks'') in the emulsion layers on both sides of the transparent plastic base. Both the position and angle of each segment were computed and recorded in real time. Efficiency for detecting microtracks was measured to be greater than 0.97.

Complete tracks were built layer by layer. Each microtrack was examined to see if it had a connectable microtrack in adjacent emulsion layers. Once reconstructed, the tracks were added to a data set unique to the given scan volume.

An important tool used in the offline emulsion data processing were high-energy muons from the beam dump that penetrated the shielding and were recorded in the scanned emulsion volume as through-going tracks with little measurable scattering, called ''calibration tracks'' below.

Data quality checks.—A systematic methodology was developed to quantify the quality of tracks found in digitized emulsion images. Two quantities were used: (a) position accuracy σ as measured by rms displacement of microtracks from fitted calibration tracks, and (b) emulsion readout efficiency ε, representing the fraction of identified calibration-track microtracks actually seen in

any one emulsion plate. Both of these quantities varied with each scanned area. Emulsion data passed the data quality check when $\sigma \leq 1.0$ μm, and $\varepsilon \geq 0.9$. Reasons for poor data quality could be a damaged emulsion (lost forever), difficulty in emulsion digitization (to be redigitized), or a systematic problem such as emulsion-sheet slipping within a stack which can be corrected as detailed below. More than 50% of the events where the predicted vertex was not initially found in the emulsion fell into the poor-data-quality category.

Emulsion-sheet slipping.—Occasionally, emulsion sheets slipped one with respect to another during exposure. An alignment method was therefore devised to correct for it using the calibration tracks. The alignment parameters of interest included the distance between the emulsion layers, the relative shifts in the transverse direction, and the shrinkage of the emulsion layers. Alignment between adjacent sheets was determined within 0.2 μm.

V. PARTICLE IDENTIFICATION

A. Muons

A muon tag was assigned to a track if there were at least four hits in the six proportional-tube planes of the muon-ID system. The per-tube efficiency for muons was measured to be 0.96, and the geometrical acceptance of the muon-ID system was estimated by Monte Carlo methods to be 0.76,
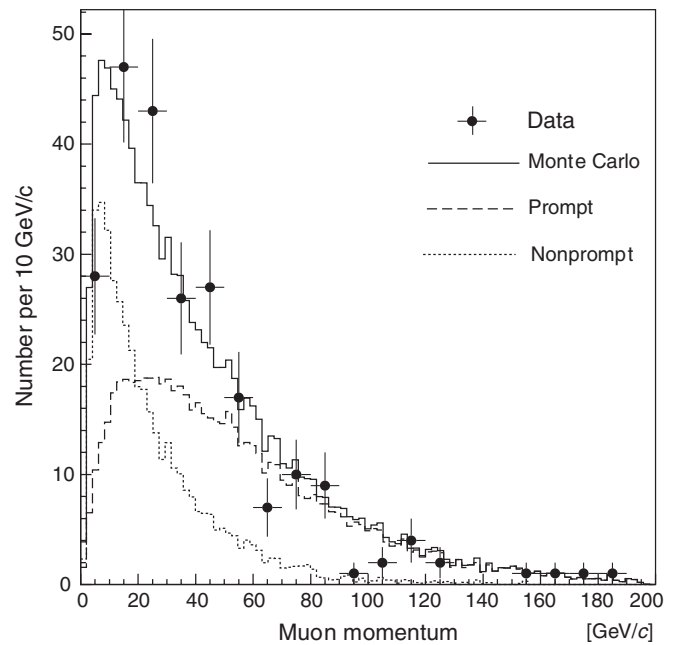

FIG. 6.   Muon momentum distribution for the set of 578 located events. The data are shown by solid circles, and Monte Carlo expectation is the solid histogram. Also shown are the expected muon distributions from the two components of the ν_μ flux, prompt (dashed line) and nonprompt (dotted line) histograms.

yielding an overall efficiency of 0.73. The muon spectra are shown in Fig. 6.

Muon track momentum could be measured in one of two very different ways: (i) from the curvature in the spectrometer, and (ii) from multiple Coulomb scattering in the emulsion.

Spectrometer measurement.—In the spectrometer, track momentum was measured using a 4 T magnet with $\int B dl = 0.75$ T m. For muons, $\Delta p/p$ was 11% for momentum p of 20 GeV/c, increasing to 100% at $p = 250$ GeV/c.

Emulsion measurement.—The high spatial precision of the tracking in emulsion, in conjunction with an adequate sampling rate, allowed the calculation of track momentum from the visible scattering of the track's segments (microtracks) in individual emulsion plates.

A special emulsion track scan was performed on all tracks found in candidate neutrino events for the dual purpose of the multiple Coulomb scattering measurement and electron identification (see Sec. V B 1). Momentum was successfully measured using multiple Coulomb scattering for 64% of the tracks in the sample.

The method was validated by test-beam experiments which showed that the beam momentum of 0.8 and 1.5 GeV/c (4 Gev/c) could be measured by the emulsion with a resolution of 23% (30%) [6,10]. A comparison of track momenta measured with both the emulsion and a spectrometer is shown in Fig. 7.

The upper limit of the momentum measured this way was determined by the number of samples, the angle of the track, the quality of the emulsion data, and the type of emulsion module. A typical upper limit was 25 GeV/c.

B. Electrons

1. Electron identification

The electron analysis was less straightforward since it involved several systems. Since the emulsion modules were two to three radiation lengths thick, most events containing electrons would exhibit showers in the SFT and in the electromagnetic calorimeter. These two electronic detectors were used to find the most likely initial energy of the electron from an algorithm using both energy (pulse height) and geometrical shower development. Shower development within the emulsion modules was simulated with the Monte Carlo method and the response was modeled using total pulse height and transverse width per SFT station as parameters. An electromagnetic signature was derived and applied to all identified showers in the data. Monte Carlo neutrino interactions, weighted to reflect the expected number of CC and NC interactions of all three neutrino flavors, were used to calculate tagging efficiency. The efficiency for electron tagging using the spectrometer was estimated to be 0.80 ± 0.04 with a purity of 0.88. Figure 8 shows the the electron-identification efficiency as a function of energy.

Electron identification using only emulsion data was attempted for all located events that did not contain a muon. A special electron-ID scan was performed on all
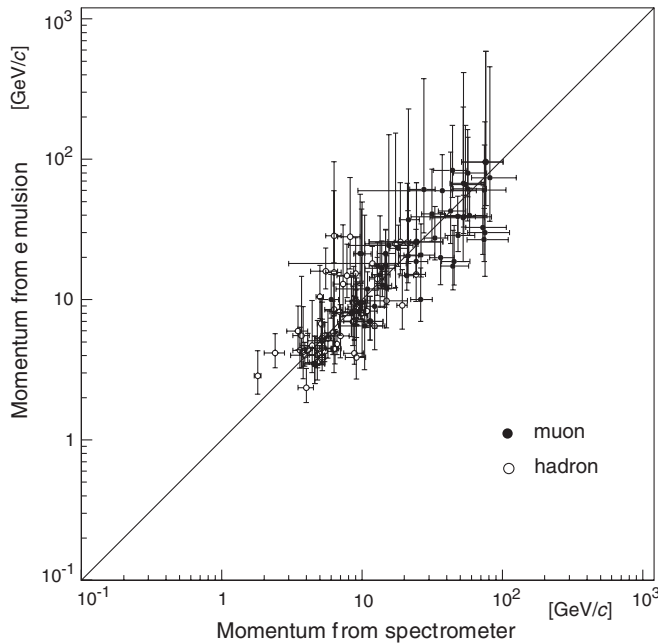

FIG. 7. A comparison between track momenta measured by multiple Coulomb scattering in emulsion and by the spectrometer. Although the tracks tagged as muons avoid secondary interactions, the momenta are often at an upper limit of measurement in the emulsion.
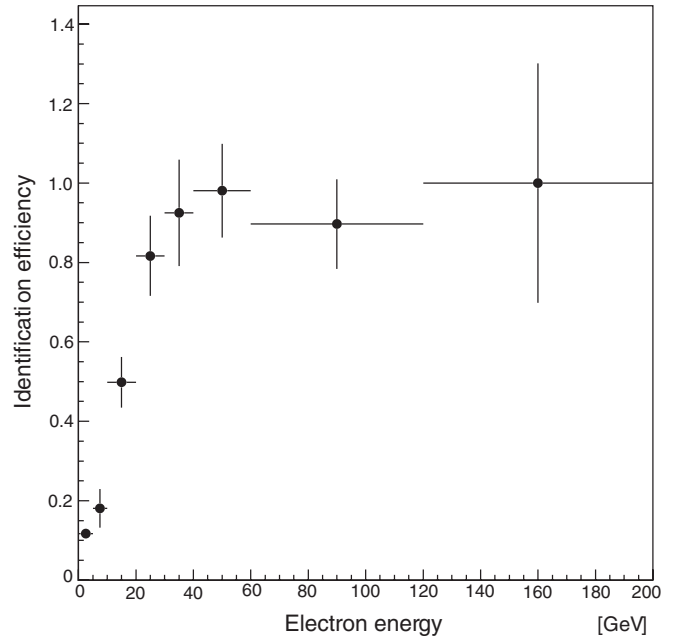

FIG. 8. The electron-identification efficiency as a function of electron energy. This analysis used the scintillating fiber detector and the calorimeter.

emulsion tracks. This scan followed each track from the vertex to the most downstream plate. An area of 600×600 μm^2 centered on the track was digitized in each emulsion plate. Electrons were identified by electron-positron pairs found within 20 μm of the track. The electron-ID scan was most effective for vertices located in the upstream part of an emulsion module. The electron tagging efficiency using emulsion data varied with path length, with a maximum of 0.86 for tracks passing through at least 2 X_0. The integrated efficiency of identifying an electron in the emulsion was 0.66.

2. Electron energy measurement

The target/fiber system was also used to estimate the electron (or gamma) energy. Since the scintillating fiber system response was calibrated to minimum-ionizing particles, the total pulse height in a shower could be summed for each station providing a direct measurement of energy. The energy estimates at each station were input variables for an algorithm to compute electron energy from shower development. The calorimeter information was added for showers that penetrated less than six radiation lengths of emulsion (approximate shower maximum). Comparison of the energy input from Monte Carlo electrons to the estimated energy from the algorithm yields the estimated energy resolution, $\Delta E/E$, of 30%.

Since the beam line could not be configured for transport of electrons, electron identification and energy estimate relied heavily on Monte Carlo simulation. A selection of probable electrons from interactions in the most downstream emulsion-target module, analyzed for momentum in the spectrometer and energy in the calorimeter, showed that the calorimeter calibration was consistent with a calibration method using muons as minimum-ionizing particles.

VI. MONTE CARLO SIMULATION

The production of neutrinos in the beam dump, their transport through the shielding system, and their interactions in the emulsion target were simulated with a GEANT3-based Monte Carlo software. The emulsion target and all electronic detectors in the spectrometer were simulated, taking into account their measured efficiencies and other response characteristics peculiar to each system.

Charmed particles produced by 800 GeV protons in the beam dump were generated using the phenomenological formula,

$$\frac{d^2\sigma}{dx_F dp_T^2} = Ae^{-bp_T^2}(1 - |x_F|)^n, \qquad (7)$$

where x_F is Feynman x and p_T is transverse momentum. The values of n in Eq. (7) depend on the charm species, but we assume that b does not. Refer to the Appendix for details of how charm production was implemented in the

analysis. The details of the simulation of neutrino production in the beam dump via charm particle decays are given in the Appendix. If the path of a neutrino originating from a charm decay intersected the emulsion target, a deep-inelastic neutrino-nucleon interaction was generated using LEPTO v6.3.

The values for n for charm production, Eq. (7), could not be determined from external data at this time. Estimates for the values of n for D_s, D^0, and $D^\pm$ production were obtained from fitting the x_F form of the above equation to output from PYTHIA (6.129) [11]. The default values for the parameters and switches in this package were not changed.

The simulated particles from the interaction were recorded in each detector and ''digitized'' as appropriate for electronics used in the experiment. These Monte Carlo data were stored in the format used by the data acquisition system and were analyzed in the same manner as experimental data. In addition, a separate file was generated with data from the charged particles within the emulsion sheets. The data contain microtracks in each emulsion layer, but they do not directly simulate the algorithms used in the UTS emulsion digitizers.

The Monte Carlo method was the primary tool for computing acceptance of the neutrino flux in the emulsion target needed for the cross section analysis. It was also used to establish selection cuts, develop electron-identification algorithms, and probe systematic effects from charm particle production uncertainties.

VII. EVENT LOCATION IN THE EMULSION

Two methods were used by DONuT to locate neutrino-interaction vertices in the emulsion target, both starting with extrapolation of spectrometer tracks back to the emulsion target. The primary method, called ''Netscan,'' used the interaction vertex position from SFT tracks to give an emulsion volume, $5 \times 5 \times 15$ mm^3, most likely to contain the event. All microtracks found within this volume were recorded for subsequent track recognition analysis. The second method used the SFT only to get an estimate of the transverse position of the vertex. In events where tracking in the SFT was difficult (e.g., showers), microtracks found in the CS at the downstream end of each emulsion module were tested for vertex formation within the target volume. Since the CS had only one-tenth the track density of the main emulsion-target sheets, the combinatoric background of false vertices was reduced. This second method was also useful for interactions yielding only one or two charged tracks, but was not used for events with accurate spatial predictions from the SFT.

A. Event location by Netscan

Netscan event location was a multistep process. Initially, information from the electronic detectors was used to fit charged-particle tracks, and reconstruct a neutrino-

interaction vertex whenever possible. The resolution of these detectors enabled vertex predictions with a precision of about 1 mm transverse and 5 mm along the neutrino beam direction. Next, both the position and size of the scanning volume were determined using the spectrometer prediction, and all microtracks within the scanning volume were digitized.

After the necessary alignment of the emulsion data, track pairs were examined to see if they formed a vertex. The following selection criteria were applied:

(i) Tracks must start within the volume and cannot be connected to any aligned microtracks in two adjacent upstream emulsion layers to reject penetrating muon tracks.

(ii) Tracks must be constructed from at least three microtracks and have a good χ^2 fit. These requirements reduce the number of low momentum tracks.

(iii) The remaining tracks were tested for vertex topology. Tracks were associated when the impact parameter at the best vertex position was less than 5 μm.

Out of the total of $\sim 10^4$–10^5 microtracks per $5 \times 5 \times 15$ mm^3 emulsion volume, only a few vertex candidates remained after the three requirements were imposed. To confirm a vertex candidate, (i) the emulsion plates near the vertex point were examined by a physicist using a manually controlled microscope to check for consistency of the neutrino-interaction hypothesis (i.e., neutral particle interaction), and (ii) the emulsion track information was compared with the hits in the SFT to verify that all tracks were associated with the same event. For interaction vertices that passed all the checks, all tracks in the event were refit using the emulsion information.

B. Event location using changeable sheets

The CS were used when the vertex prediction was problematic: the event was either too complex to have an accurate vertex prediction made, or, on the other hand, only one charged track was reconstructed in the SFT, so that the interaction point was constrained only in the two transverse dimensions. In this case, the SFT track was extrapolated to the CS position and the emulsion data in this sheet were searched for a track matching both position and angle. If found, the track could be followed into the emulsion-target module with much greater accuracy to greatly reduce ambiguity in high track-density regions. The SFT-CS matched tracks were followed upstream, through the sheets of the target module, using emulsion scanning within a cylindrical volume (used in Ref. [4]) or within a conical volume with transverse dimensions increasing along the track. The latter scan resulted in much larger emulsion volume being scanned to increase event location efficiency, but also greatly increased the digitizer work load. This was only possible when UTS digitizers became available in the

year 2000, one and one-half years after the emulsion analysis began.

If a track penetrated all the way to the most upstream sheet, the track was rejected. If the track was found to be missing in upstream sheets, it was assumed to originate in the space between emulsion layers. All tracks followed in this way were checked to ensure that they did not originate as an $e^+ e^-$ pair, a secondary interaction, or as an emulsion inefficiency causing a gap in a through-going track. Electron-positron pairs were recognized as either (a) two minimum-ionizing particles separated by 5 μm or less and with an angular separation of less than 10 mrad, or (b) a track consistent with an ionization greater than one minimum-ionizing particle. In either case, the track(s) did not originate at the primary vertex. If these background hypotheses were rejected, the track was assumed to originate from a primary vertex of a neutrino interaction. All other emulsion tracks that passed within 5 μm of this track's endpoint were checked visually to see if they were likely to originate in the same interaction, perhaps due to a digitization error.

C. Special cases

Special methods were developed for events with a large number of hits in SFT, for which the total pulse height exceeded the equivalent of 650 minimum-ionizing tracks and no 3-D tracks could be reconstructed. These large-pulse height events are called *LP events* below.

In the *modified CS scan*, a large area (> 1 cm^2) was scanned in the CS nearest to the upstream end of a large SFT shower, and an electron signature was searched for in the form of clustered parallel microtracks. If found, the electron was followed upstream to the vertex. Alternatively, a line was drawn through the shower core in the SFT to better pinpoint the CS area to be scanned, with a typical size of 5×5 mm^2. In this case, no electron signature was required, and all tracks matching the line in position and angle were followed back.

In the *modified Netscan*, a number of lines were drawn in u and v projection and extrapolated into the emulsion module. If a candidate vertex region was found, Netscan was applied to an oversized volume, typically $13 \times 13 \times 20$ mm^3.

The two methods yielded a similar numbers of events, with a total of 58 LP events located in the emulsion, of which 31 were ν_e events, 9 ν_μ events, 2 ν_τ events, and 16 NC events.

D. Location efficiency

The overall efficiency for locating the primary vertex in the emulsion was given directly as the ratio of the number events found and the total number of events for which a vertex prediction was made and then scanned. This ratio is $578/866$ or 0.667 ± 0.036.
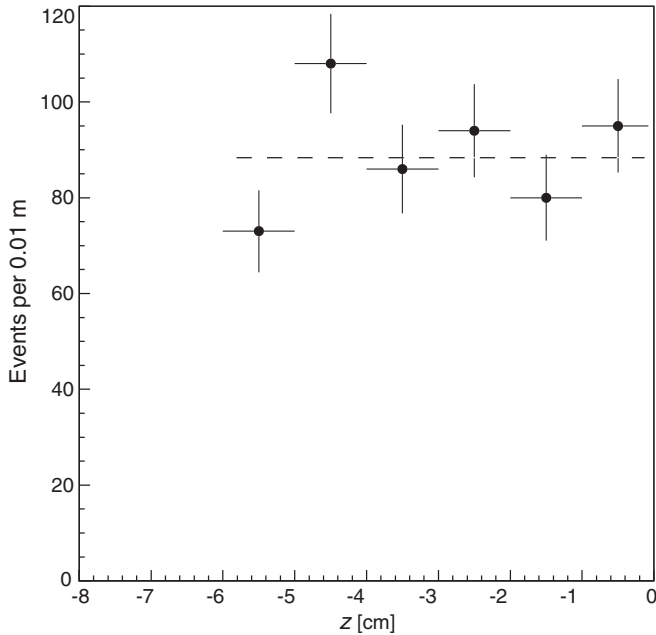
FIG. 9. Number of located events as a function of z, the vertex position measured from the downstream edge of a module along the beam direction. Data from all seven modules are included. Also shown (dashed line) is the fit assuming the results are independent of z, yielding a value of 88 with χ^2/dof equal to 1.7.

We note that each module corresponded to 2.5 to 3 radiation lengths and 0.2 interaction lengths, so secondary interactions were a common occurrence. Resulting large hadron/electromagnetic showers hampered track recon-
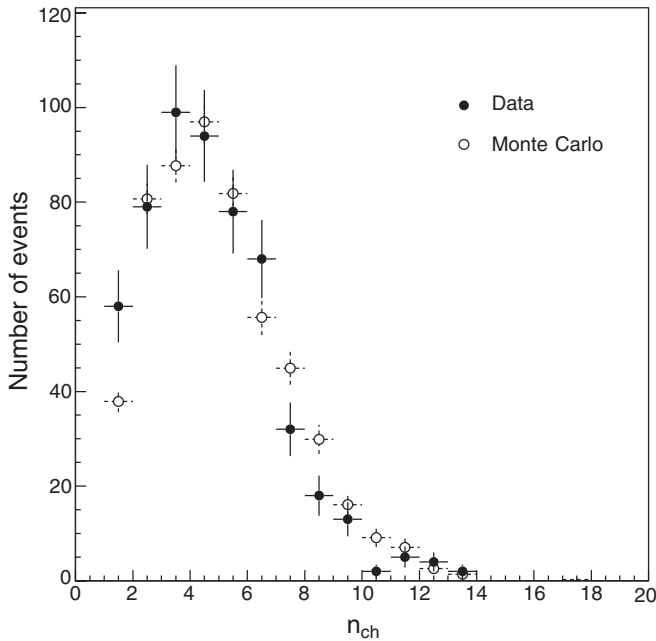

FIG. 10. Charged-particle multiplicity, n_{ch}, at the primary vertex of all the located events. Data are shown by solid circles, Monte Carlo data by open circles.

struction and vertex location. There were 188 events classified as LP events, or 22% of the total of 866. A total of 58 LP events were located in the emulsion, representing a location efficiency of 0.31 ± 0.05, to be compared to 0.77 ± 0.04 location efficiency for the regular events (520 located out of a total of 678).

We investigated the located-event sample for possible biases. Figure 9 displays the distance along the beam direction between the vertex and the downstream edge of an emulsion module, for all 7 modules. The distribution is consistent with being independent of z, with χ^2/dof to a straight line of 1.7. The vertex distribution in the transverse plane (not shown) is uniform, as expected. The located-event charged multiplicity distribution is compared with expectation in Fig. 10. We conclude that the benefit of using a combination of different location methods was to have uniform location efficiency.

VIII. SECONDARY-VERTEX ANALYSIS

A. Decay search criteria

For the located events, the emulsion was digitized again in a smaller volume containing the vertex and optimized for the decay search, typically $2.5 \times 2.5 \times 12$ mm^3. The track reconstruction algorithm was the same as that used for vertex location. The decay search was divided into two categories distinguished by topology:

(1) *Long-decay search:* Decays in which the candidate parent track passed through at least one emulsion layer.

(2) *Short-decay search:* Decays in which only the daughter track was recorded in emulsion.

The strategy was common for both decay topologies under consideration. Once a secondary vertex was found, the event was classified as a one-prong decay, unless additional tracks were found to be associated with the same secondary vertex constituting a three-prong decay.

Tau and charm decays were obtained from the data in a two-step process: (i) finding secondary vertices in emulsion data using geometrical cuts, described in this section, and (ii) subsequently imposing topological and kinematical cuts to isolate the signal from the background, described in Sec. VIII B.

1. Long-decay search

The long-decay search for one-prong decays imposed the following criteria:

(i) The parent track had one or more microtracks, and a daughter track had three or more microtracks.

(ii) The parent-track length: $L_{dec} < 10$ mm.

(iii) The impact parameter b_p of the parent track with respect to the primary vertex (as defined in Sec. VII A: (i) $b_p < 5$ μm if there were at least two microtracks, or (ii) $b_p < (5 + 0.01 \times \delta z)$ μm

if there was one microtrack, where δz is the distance from the parent microtrack to the vertex.

(iv) The minimum distance, $d_{\min}$, between extrapolated parent and daughter tracks: (i) $d_{\min} < 5$ μm if there were at least two parent microtracks, or (ii) $d_{\min} < (5 + 0.01 \times \delta z)$ μm if there was only one parent microtrack.

(v) (i) The angle between the daughter and parent tracks: $\alpha > 4$ times the angular measurement error, or (ii) the impact parameter b_d of the daughter with respect to the primary vertex: $b_d > 4$ times the error in the position.

Candidate tracks passing the above criteria were checked in the emulsion by a physicist using a microscope for the following three requirements. First, to ensure that the daughter track could not be associated with emulsion tracks upstream of the vertex, the two sheets immediately upstream of the vertex were examined for tracks at the projected location of the candidate track. If an upstream track was found within 20 μm of the position and 10 mrad in angle of the candidate projection, it was rejected. Second, the candidate track was examined to see if it was a part of a e^+e^- pair. If another track was observed within 120 μm of the candidate track and began in the same sheet as the candidate track, then it was tagged as a possible pair. Then, the electronic emulsion data were checked in a cylindrical volume of 30 μm radius centered on the candidate track. If there were any more tracks in this cylinder with an angle within 20 mrad of the candidate, it was rejected as a likely e^+e^- pair. And third, the area in the sheets within 100 μm of the candidate was examined for alignment problems, since poor calibration could mimic a kink. This was checked with through-going background tracks from high momentum muons.

2. Short-decay search

The short-decay search for one-prong decays required the following criteria:

(i) The daughter track had at least three microtracks.

(ii) The daughter-track impact parameter (IP) with respect to the primary vertex: $b_d < 200$ μm.

(iii) The daughter-track IP with respect to the primary vertex: $b_d > 4 \times \sigma_{\mathrm{IP}}$, where σ_{IP} is the error on the impact parameter.

Each candidate daughter track was checked visually to insure that it could not be connected to microtracks upstream of the vertex.

B. Tau and charm recognition

To extract the ν_τ signal from events passing the secondary-vertex selection, a set of topological and kinematical criteria was first applied as described in Sec. VIII B 1 below. In the second step, the amount of signal and background was determined using a multivariate technique featured in Sec. VIII B 2.

1. Topology and kinematical cuts

ν_τ *event topology.*—The ν_τ CC interactions, reaction (1), produce a τ lepton that typically decays within 2 mm of its origin. Thus, the topological signature for ν_τ events is a track from the primary vertex that gives a secondary vertex at a short distance consistent with the kinematics of the decay. There must be no other lepton from the primary vertex. The topological signature of charm production in reaction (5) is very similar to ν_τ events. Tau and charm events were distinguished primarily by the presence of an electron or muon at the interaction vertex. Thus, a ν_e or a ν_μ CC interaction together with a failure in lepton identification constitutes the primary background to the tau sample. The second background considered here were interactions of hadrons produced in neutrino NC interactions, reaction (6), that appeared in the emulsion with a topology of a one-prong or three-prong interaction (or decay).

Kinematical cuts.—The following set of criteria were derived from Monte Carlo studies to efficiently extract the ν_τ signal with minimal background. It is a modified version of the selection criteria of Ref. [4]. Long one-prong and trident decays were accepted when the following conditions were satisfied:

(i) Parent-track angle with respect to neutrino direction: $\theta_p < 0.2$ rad.

(ii) Daughter-track angle with respect to parent direction: $\theta_d < 0.3$ rad.

(iii) Kink angle: $\alpha < 0.25$ rad.

(iv) Daughter-track IP: $b_d < 500$ μm.

(v) Transverse momentum of the daughter with respect to parent track: $p_T > 250$ MeV/c for hadrons, and $p_T > 100$ MeV/c for electrons and muons.

(vi) Daughter momentum: $p_d > 1$ GeV/c.

Events passing these criteria that did not have an identified electron or muon track from the primary interaction vertex were selected as ν_τ candidate events. In the case of trident secondary vertices, at least one of the secondary tracks must pass all of the above requirements. Figure 11 shows the distribution of the number of kinks versus transverse momentum, p_T, of the daughter with respect to the parent track, for all tracks satisfying the above criteria except the transverse momentum cut. One can see that p_T is an impressive discriminant. There are 198 tracks, but almost all are within the steeply falling peak at low p_T due to hadronic background, reaction (6). All but one of the other tracks are classified as either tau or charm decays following the multivariate analysis outlined in the next section.

For short decays, all the cuts were the same but one: the kink angle α cannot be defined since the parent direction is unknown. Here the kink angle was replaced by the "minimum kink angle," obtained by extrapolating the daughter track back to the steel plate and placing the "decay vertex" at the point where this extrapolation intersects the down-
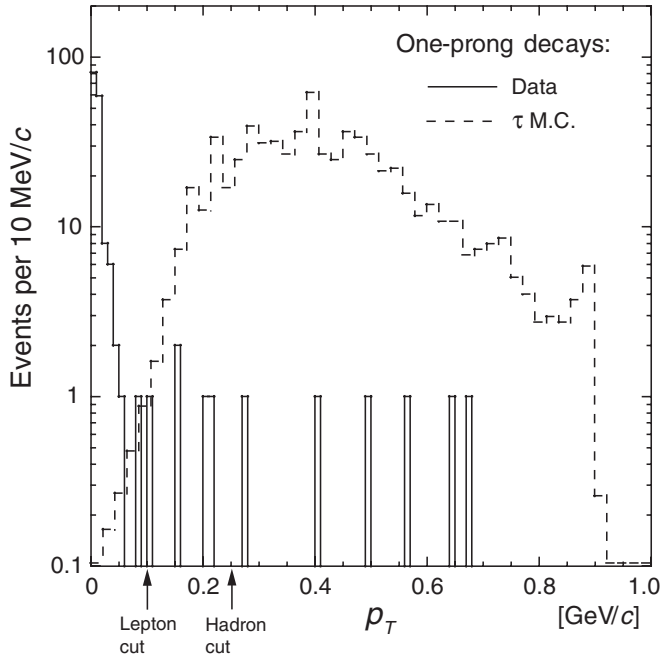
FIG. 11. The distributions of one-prong secondary-vertex events (solid line) after all the topological and kinematic cuts *except* on transverse momentum. Superposed is the expected distribution from τ one-prong decays (dashed line, arbitrary normalization). For τ candidates, the kink transverse momentum must exceed 0.25 GeV/c for $\tau \rightarrow$ hadron or exceed 0.1 GeV/c for $\tau \rightarrow e$ or μ.

stream face of the plate. This was the most conservative assumption, since it also minimized the transverse momentum assigned to the decay.

2. Multivariate analysis

Only events selected by secondary-vertex analysis detailed above were submitted to the multivariate analysis employed to determine the probability that individual events represented one of the following interaction types, each with a one-prong or a three-prong secondary vertex:

(1) ν_τ CC events, reaction (1).
(2) Charm production, reaction (5).
(3) Neutrino NC events with a secondary hadron interaction, reaction (6).

No other physical process, subject to the topological and kinematical cuts above, was deemed to be a significant part of the background.

A set of quantities was chosen that could be easily and unambiguously measured in the emulsion data (supplemented by spectrometer information) and that could discriminate between the three hypotheses. Note that all these quantities are independent of the neutrino production and interaction processes. For n parameters, an n-dimensional probability density distribution for each hypothesis was computed using Monte Carlo generated events. Then the relative probability of event k sampled from the distribution of hypothesis i can be written as

$$P(\{x_k\}|i) = \frac{\mathcal{W}_i \mathcal{P}(\{x_k\}|i)}{\sum_j \mathcal{W}_j \mathcal{P}(\{x_k\}|j)}, \qquad (8)$$

where $\{x_k\}$ is a set of parameters describing event k, $\mathcal{P}(\{x_k\}|i)$ is the probability density function for hypothesis i evaluated for x_k determined from the data, and $\mathcal{W}_i$ is the prior probability of the event being an i-type event. Note that the $\mathcal{W}_i$ are independent of $\{x_k\}$, and give the probability of a neutrino interaction of type i occurring within the emulsion fiducial volume using full Monte Carlo simulation starting with neutrino production in the beam dump through its interaction in the emulsion target.

The parameter set $\{x_k\}$ for events selected as tau candidates included L_{dec}, α, p_d, θ_p, and $\sum b_d$, introduced above. In addition, $\Delta\phi$ was added, which represents the angle in the plane transverse to the neutrino beam between the parent direction and the vector sum of unit vectors of the remaining tracks at the primary vertex, expected to peak at 180° for ν_τ CC events, and to distribute uniformly for the other two hypotheses.

Hence, for one-prong decay candidates resulting from the long-decay search, the set $\{x\} = \{L_{\text{dec}}, \alpha, p_d, \theta_p, \Delta\phi\}$

FIG. 12. An example of simulated distributions used as input to the event probability calculation within the multivariate method as applied to all decays. Shown are distributions of the transverse-plane angle $\Delta\phi$ for all three hypotheses under consideration: tau (solid line), charm (dashed line), and hadronic interactions (dotted line). Short vertical lines indicate the values for ν_τ candidate events from Table V for one-prong decays (solid line) and three-prong decays (dashed line)

FIG. 13. An example of simulated distributions used as input to the event probability calculation within the multivariate method as applied to one-prong decays. Shown are distributions of the kink angle α for all three hypotheses under consideration: tau (solid line), charm (dashed line), and hadronic interactions (dotted line). Short vertical lines indicate the values for ν_τ candidate events from Table V.
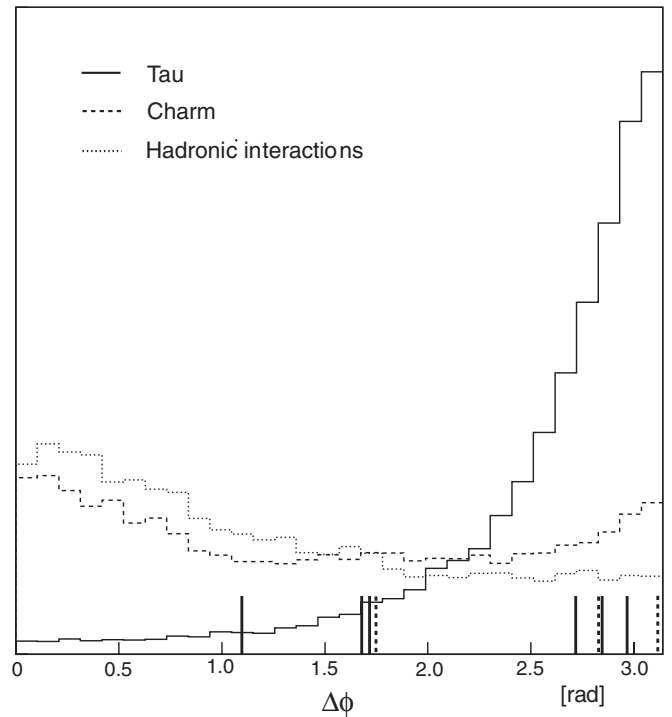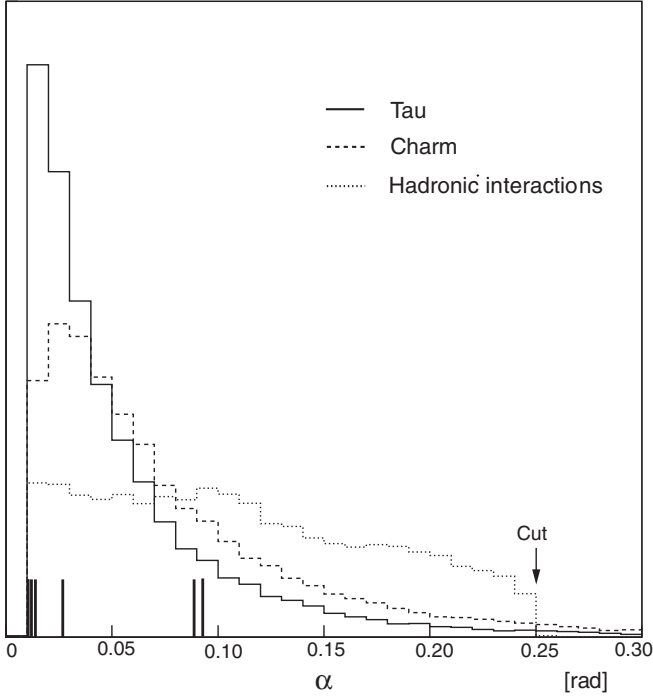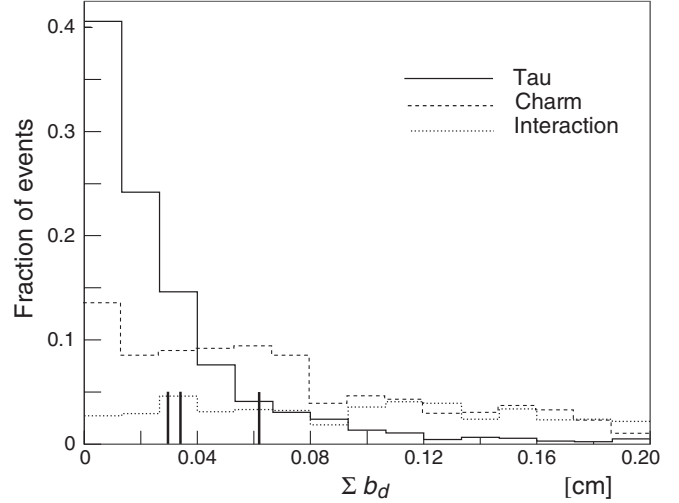

FIG. 14. An example of simulated distributions used as input to the event probability calculation within the multivariate method as applied to three-prong decays. Shown are distributions of $\sum b_d$, the sum of daughter-track impact parameters for all three hypotheses under consideration: tau (solid line), charm (dashed line), and hadronic interactions (dotted line). Short vertical lines indicate the values for ν_τ candidate events from Table V.

was used, and $\{x\} = \{L_{\text{dec}}, \theta_p, \Delta\phi, \sum b_d\}$ was used for three-prong decays.

Simulated distributions used as input to the multivariate method are illustrated in Figs. 12–14 for all three hypotheses. Figure 12 shows the $\Delta\phi$ angle in the transverse plane, used for both one- and three-prong topologies, which discriminates strongly against both charm and hadronic-interaction background. Figure 13 shows the α decay angle used for the one-prong topology, which discriminates against the hadronic-interaction background, and provides modest discrimination against charm. Figure 14 shows $\sum b_d$, the sum of the daughter-track impact parameters, used for the three-prong topology. This quantity is related to ct for this event, where t is this parent's lifetime in its rest frame. Since τ lepton has a shorter lifetime than charmed mesons, $\sum b_d$ discriminates strongly against the hadronic-interaction background, and provides discrimination against charm. Note that these one-dimensional distributions do not provide information about correlations among the multivariate parameters which are taken into account in the calculation.

The multivariate analysis was also used for events from the short-decay search. Here, the parent direction is unknown, and hence θ_p, α, and $\Delta\phi$ are unknown. The true decay point must have been in the same steel plate that

contained the interaction vertex, lying on a line made by projecting the candidate daughter track upstream. Along this line within the steel, the parameters L_{dec}, α, θ_p, and $\Delta\phi$ vary continuously, so that probabilities for the three hypotheses also vary. To make a definite and conservative estimate, the values of all three probabilities were measured at the point along the line where the tau-hypothesis probability was minimum.

Table I summarizes the prior probabilities for both kink and trident topologies and different materials of the emulsion target. Resulting hypothesis probabilities for the ν_τ event candidates are presented in Sec. IX D.

C. Decay search efficiencies

The effect of cuts applied during the secondary-vertex search was determined by Monte Carlo calculation for all three hypotheses, tau, charm, and hadronic interaction. The secondary-vertex search efficiency was checked by using secondary hadronic interactions found as a byproduct of the track-by-track electron-ID scans. The number of interactions expected has a well-understood value depending on path length in a given material (emulsion, steel, or plastic). The number of interaction vertices of any multiplicity was estimated to be 31. The total number of found interactions was 27, yielding an efficiency of 0.87, consistent with a Monte Carlo derived efficiency of 0.86.

The fractions of events remaining after selections described in Secs. VIII A and VIII B 1 are listed in Table II. Variations in the emulsion track efficiency in a scan area affected the ability to estimate these efficiencies with the

TABLE I. Summary of the prior probabilities for the multivariate analysis.

Material	No. of decay prongs	Prior probabilities $\mathcal{W}$		
		Tau decay	Charm decay	Hadron int.
Emulsion	1	2.7×10^{-3}	1.9×10^{-3}	4.1×10^{-5}
Emulsion	3	2.7×10^{-3}	1.9×10^{-3}	2.0×10^{-4}
Plastic	1	1.6×10^{-2}	1.2×10^{-3}	7.5×10^{-6}
Plastic	3	2.7×10^{-3}	1.9×10^{-3}	6.7×10^{-5}
Steel	1	1.6×10^{-2}	1.2×10^{-3}	5.1×10^{-4}
Steel	3	1.6×10^{-2}	1.2×10^{-3}	5.6×10^{-3}

TABLE II. Efficiencies for identifying the secondary vertex in ν_τ interactions, in charm-producing ν_e and ν_μ interactions, and in ν NC events with secondary hadronic interactions. (A kink-daughter type is given in parentheses.)

Decay topology	$\nu_\tau \rightarrow \tau^-$	$\bar{\nu}_\tau \rightarrow \tau^+$	$\nu \rightarrow$ charm	$\bar{\nu} \rightarrow$ charm	Hadron interactions
1-prong (hadron)	0.39	0.39	0.26	0.32	0.72
1-prong (electron)	0.49	0.51	0.35	0.36	
1-prong (muon)	0.50	0.54	0.34	0.33	
3-prong decay	0.58	0.62	0.45	0.56	0.84
All	0.46	0.47	0.34	0.40	0.76

Monte Carlo method. A simulation of emulsion pathologies (local inefficiency and distortion) gave an estimate for the overall systematic uncertainties in these efficiencies of 5% of the value.

IX. SURVEY OF DATA

A. Expected composition

The expected number of interactions for reactions (2)–(4) was predicted using the DONuT Monte Carlo method simulating the same event-selection procedure that was applied to the data. Charged-current interactions of all flavors were selected by identifying a lepton at the primary vertex. All neutrino interactions without an identified lepton were considered to be "effective neutral-current" events, NC_{eff}. These NC_{eff} events therefore included CC events with a lepton that escaped detection. Table III shows the expected number of events of all four interaction types. Note that although the prompt and nonprompt components

(see Sec. II) are separated in the simulation, they are not distinguishable in the data.

B. ν_μ CC events

The identification of muons using the spectrometer was straightforward and efficient, so this category of interactions was considered the most reliable. The number of ν_μ CC events found was 225 events, which gives the fraction of ν_μ CC to the total (578) as 0.39 ± 0.03.

The fraction of nonprompt ν_μ CC events was estimated both by the Monte Carlo method and from the data using three distinct methods. First, a stand-alone GEANT-based Monte Carlo simulation of 800 GeV proton-nucleon interactions was employed to record all the hadronic cascade pions and kaons with energy greater than 5 GeV. These simulated secondaries in the beam dump were forced to decay leptonically to estimate the nonprompt neutrino flux. The second method used the DONuT Monte Carlo simulation to compute the prompt ν_μ flux and the resulting

TABLE III. Expected composition of the beam dump neutrino beam. The distinction of ν_μ from prompt (charm decay) and nonprompt (π and K decay) sources is made only for Monte Carlo generated events. The NC_{eff} category includes all events not classified as charged current. The number of data events are not corrected for background.

	ν_e CC	ν_μ CC Prompt	ν_μ CC Nonprompt	ν_τ CC	NC_{eff}
MC fraction	0.190	0.208	0.163	0.018	0.421
MC fraction $\times$ 578	110	120	94	10	244
Data	120	225		9	224
Difference	10 ± 11	11 ± 15		-1 ± 3	-20 ± 15

spectrum of muons from ν_μ CC interactions. This spectrum was subtracted from the measured spectrum obtained from the 225 data events containing muons, yielding the nonprompt estimate. The third method used data obtained using a "half-density" beam dump, in which the tungsten was removed every 2.5 cm along the proton beam direction. The results from these three analyses give the prompt fractions 0.62 ± 0.05, 0.51 ± 0.10, and 0.67 ± 0.16, respectively. The weighted mean is 0.61 ± 0.04. The estimated number of prompt ν_μ CC interactions is thus 137 ± 13.

The ratio of the number of $\bar{\nu}_\mu$ interactions with outgoing μ^+ to the number of ν_μ interactions with μ^- was computed from ν_μ and $\bar{\nu}_\mu$ cross sections taking into account detector efficiency and acceptance. The resulting expected ratio was 0.63. The same ratio from the data sample was 0.67 ± 0.08. Using this measured number, the ratio of integrated $\bar{\nu}_\mu$ and ν_μ fluxes was found to be 1.05 ± 0.13.

There are three events in the located sample that have two identified muons. One event has muons of opposite sign with one from the primary interaction vertex and the other from a secondary decay vertex. This event is identified as a ν_μ CC interaction producing a charmed meson. The other two dimuon events have same-sign tracks, where one of the tracks is likely a charged π decaying in flight.

C. ν_e CC events

The expected mean energy of outgoing electrons in ν_e CC interactions was 52 GeV, with 22% of events having electron energies below 20 GeV. Approximately 15% of NC events have at least one electron with energy less than 20 GeV. Therefore, a low-energy cut is applied to the electron sample to reduce background from events that are not ν_e CC events. Table IV summarizes the result of a Monte Carlo-based study to optimize this cut and to estimate the NC background as a function of energy. For cuts of 18 GeV and higher, there is little change in signal-to-background ratio and a cut of 20 GeV was chosen. A total of 120 ν_e CC and NC_{eff} events passed the cut. The NC_{eff} background fraction is estimated in Table IV to be

0.174, so the number of ν_e CC events without background (with a 20-GeV electron cut) is estimated as $120 \times (1 - 0.174) = 99 \pm 9$, as determined by the electronic detector data. To compare this number to the second identification method which follows, it must be divided by the electronic tagging efficiency (0.80, Sec. V B 1), yielding 124 ± 11.

The set of events with electrons identified in the emulsion (Sec. V B 1) was a second, independent, estimate of the number of ν_e CC events. There were 82 events with primary electrons found in the emulsion data alone. Of these, 62 electrons passed the 20 GeV minimum energy cut. The electron-identification efficiency of this procedure was found to be independent of energy. The number of ν_e CC, corrected by the efficiency, was $62/0.66 = 94 \pm 12$.

D. ν_τ CC events

The methods of selecting the ν_τ events described in Sec. VIII were applied to the 578 located events. The multivariate analysis (Sec. VIII B 2) was performed for each selected event. Events with $P(\tau) > 0.5$ are listed in Table V. We estimate the number of ν_τ, charm, and hadronic-interaction events in our final sample by summing up the hypothesis probabilities in Table V, yielding 7.5 ν_τ events, 1.26 charm events, and 0.22 hadronic interactions. The value of 7.5 ν_τ CC interactions is used as the best estimate for the cross section results in Sec. X.

Input values used in the ν_τ cross section analysis, including charm cross sections are listed in Table VI.

The charm and hadronic-interaction backgrounds can also be estimated in the tau sample using one-dimensional cuts on Monte Carlo events without any reference to the correlations between variables. This simpler analysis gives an estimate of the background from charm decays and hadronic interactions in the nine selected events as 1.1 and 0.9 events, respectively. In comparing the results between the two analyses, it is important to note that the multivariate method accounts for correlations between parameters and results depend on the particular set of candidate events. This last point is significant due to the small number of tau events. The similarity of the charm background from the two analyses demonstrates the simi-

TABLE IV. Results of a systematic study of classifying ν_e CC events as a function of electron energy. N_e^{data} includes both ν_e CC events and a background of NC_{eff} events misidentified as ν_e CC events. The last column gives the estimated true number of CC ν_e events after subtracting background and correcting for efficiency, and should be constant in energy if systematics are small. Events with energy less than 20 GeV were rejected from the CC ν_e set and therefore assigned to the NC_{eff} set.

Energy cut (GeV)	N_e^{data}	$N^{data}(NC_{eff})$	$\varepsilon(\nu_e CC)$	NC_{eff} bkg	N_e^{corr}
15	144	207	0.747	0.239	147
18	134	217	0.693	0.194	156
20	120	224	0.635	0.174	156
25	104	247	0.573	0.160	152
30	91	260	0.514	0.153	150

TABLE V.   List of ν_τ events with values of parameters used in the analyses and the result of the multivariate analysis.

Event	Daughter	L_{dec} (mm)	α (rad)	b_d (μm)	$\Delta\phi$ (rad)	θ_p (rad)	p_d (GeV/c)	$P(\tau)$	$P(c)$	$P(\mathrm{int})$
3024/30 175	e	4.47	0.093	416	1.09	0.030	5.2	0.53	0.47	0.00
3039/01 910		0.28	0.089	24	2.71	0.065	4.6	0.96	0.04	0.00
3140/22 143	μ	4.83	0.012	60	1.67	0.040	22.2	0.97	0.03	0.00
3333/17 665	e	0.66	0.011	8	2.84	0.016	59	0.98	0.02	0.00
3024/18 706	e	1.71	0.014	23	2.96	0.043	50	1.00	0.00	0.00
3139/22 722 [a]		0.44	0.027	12	1.71	0.155	15.8	0.50	0.29	0.21
3296/18 816		0.80	0.054	38	1.74	0.140	5.0	0.71	0.29	0.00
			0.190	148			1.3			
			0.130	112			1.9			
3334/19 920		8.88	0.017	147	3.11	0.041	11.6	1.00	0.00	0.00
			0.011	98			15.7			
			0.011	94			3.2			
3250/01 713		0.83	0.133	110	2.83	0.028	1.3	0.87	0.12	0.01
			0.192	161			2.4			
			0.442	355			0.5			
Total								7.52	1.26	0.22

[a]Event 3139/22 722 was a short decay so the probability values listed are at the tau probability minimum. Six events are kink decays and the last three listed are trident decays.

larity in the topological signature of tau and charm decays. The hadronic-interaction background, however, shows little correlation between parent-track length and "decay" (interaction) topology, and simple one-dimensional cuts overestimate this background.

E. Charm production in neutrino interactions

Integrating over the expected neutrino energy spectrum, the average charm production fraction, normalized to the number of ν_μ and ν_e CC interactions, is 0.066 ± 0.008 [12]. This fraction includes production of D^0, $D^\pm$, D_s, and Λ_c. Including only charged charmed hadrons reduces the fraction to 0.028 ± 0.006. The expected number of charged charm events is the product of the total number of located events (578), the fraction of CC events (0.62), the efficiency for observing the secondary decay (0.45 ±

TABLE VI.   Quantities used in the analysis to compute the tau-neutrino cross section. The proton-tungsten total cross section is listed as σ_{tot} (pW). The charm production cross section in a material of atomic number A is assumed to be proportional to A^α. The parameters b and n are defined by Eq. (7). Note that the value given for n was obtained from PYTHIA output.

Quantity	Value
$\sigma(\mathrm{pN} \to D^\pm X)$	21 ± 2 μb
$\sigma(\mathrm{pN} \to D^0 X)$	41.3 ± 2.6 μb
$\sigma(\mathrm{pN} \to D_s X)$	7.9 ± 1.2 μb
$\sigma(\mathrm{pN} \to \Lambda_c X)$	8 ± 5 μb
σ_{tot} (pW)	1650 mb
α	0.99 ± 0.03
n	6.1 ± 0.1
b	0.80 ± 0.10 (GeV/c)$^{-2}$

0.05), and the charged charm fraction (0.028). The result is 4.5 ± 1.0 events, where the error represents the uncertainties in cross sections and branching ratios. The observed number of charged charm events in our sample is 7 events, with an estimated background level of 2.2 events, which is consistent with our prediction.

X. NU-TAU CROSS SECTION

A. Parameter-dependent analysis

The total CC cross section per nucleon can be factored as

$$\sigma(\nu_\ell) = \sigma^{\mathrm{const}}(\nu_\ell) E K_\ell(E), \qquad \ell = e, \mu, \tau, \quad (9)$$

where $\sigma^{\mathrm{const}}(\nu_\ell)$ is the energy-independent part of the cross section of flavor ℓ, E is the neutrino energy, and K_ℓ gives the part of the neutrino cross section that depends on kinematic effects due to the lepton mass. In the DONuT energy range, the factors K_e and K_μ can be safely taken to be unity. K_τ is shown as a function of E in Fig. 15.

The ν_τ cross section for CC interactions requires measurements or estimates for the neutrino flux at the emulsion target and a total efficiency for identifying a ν_τ interaction. In general the number of observed neutrino interactions can be written as

$$N_{\mathrm{int}} = \varepsilon_{\mathrm{TOT}} N_\nu^{\mathrm{tgt}} \frac{N_{\mathrm{nucl}}}{\mathrm{area}} \sigma(\nu), \quad (10)$$

where $\varepsilon_{\mathrm{TOT}}$ is the experimental efficiency for observing the interaction, N_ν^{tgt} is the number of neutrinos passing through the area subtended by the target, $\sigma(\nu)$ is the interaction cross section per nucleon, and N_{nucl} is the number of nucleons contained in the target area.
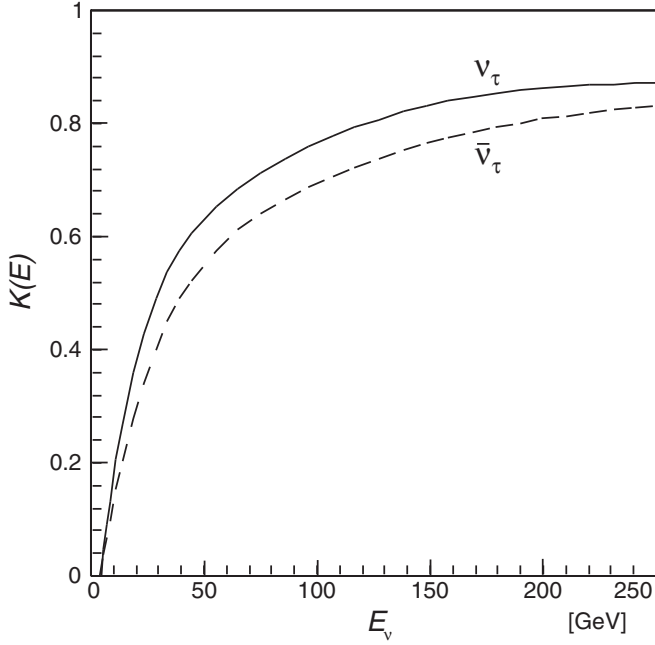
FIG. 15. The tau lepton mass suppresses the ν_τ CC cross section relative to the ν_μ and ν_e cross sections.

Specifically, we expand Eq. (10) as

$$N_{\text{int}} = \varepsilon_{\text{TOT}} R_\ell N_{\text{pot}} f_\ell \frac{M_{\text{tgt}}}{\text{area} \times m_{\text{nucl}}} \frac{\sigma^{\text{const}}(\nu_\ell)}{N_\nu^{\text{MC}}} \sum EKTt$$

$$= \sigma^{\text{const}}(\nu_\ell) \varepsilon_{\text{TOT}} C_\ell F_\ell(n), \qquad (11)$$

where the sum is over neutrinos generated with the Monte Carlo program. R_ℓ is the number of neutrinos created in the beam dump per 800 GeV proton, and N_{pot} is the integrated number of protons on target for the DONuT exposure. f_ℓ denotes the fraction of the neutrino flux intercepting the emulsion. Hence, the number of neutrinos passing through the emulsion is $N_\nu^{\text{tgt}} = R_\ell f_\ell N_{\text{pot}}$. M_{tgt} is the emulsion-target fiducial mass with $N_{\text{nucl}} = M_{\text{tgt}}/m_{\text{nucl}}$. The area is taken to be the size of the emulsion, 50×50 cm^2. The number of neutrinos generated in the Monte Carlo simulation, N_ν^{MC}, is a normalization factor for the last term.

Two additional quantities were introduced in Eq. (11), C_ℓ and $F_\ell(n)$. The quantity C_ℓ incorporates the energy-independent factors and depends on neutrino flavor:

$$C_\ell \equiv R_\ell N_{\text{pot}} \frac{M_{\text{tgt}}}{\text{Area} \times m_{\text{nucl}}}, \qquad \ell = e, \mu, \tau. \qquad (12)$$

The quantity $F_\ell(n)$ is defined by

$$F_\ell(n) \equiv f_\ell \left\langle \sum EKTt \right\rangle_\ell, \qquad \ell = e, \mu, \tau. \qquad (13)$$

The brackets indicate the mean value of the sum is used. The binary T is equal to 1 if the neutrino passed within the target fiducial volume and the binary t is equal to 1 if the

interaction generated a trigger. For the Monte Carlo events, the simulated trigger also incorporated the muon identification for ν_μ interactions. The electron identification, with its efficiencies, was not incorporated directly into t but it was incorporated into ε along with other electronic and analysis efficiencies.

The quantity $F_\ell(n)$ was computed using the Monte Carlo method, with values for b and n of Eq. (7). It is equal to the mean energy of the neutrinos that interact and trigger the experiment. We assume that the transverse dependence of charm hadroproduction is the same for all charm species. The longitudinal dependence is known to be sensitive to quark content as well as energy. Therefore, we do not make the assumption that n is the same for all charm production. Instead, it is carried along as a parameter of the analysis and the number of neutrino interactions is quantified as a function of n. The values of C_ℓ and F_ℓ used in this analysis are listed in Table VII. F_e and F_μ are used only for estimating the number of ν_e and ν_μ interactions. (See the Appendix for details.)

It is important to note that total charm cross section data exist (Table VIII), so that R_ℓ may be calculated. But data on the longitudinal dependence of the cross sections for charm, D_s in particular, are not available. $F_\ell(n)$ contains the effects of this dependence.

From Eq. (11), the ν_τ cross section is computed from the following expression:

$$\sigma^{\text{const}}(\nu_\tau) = \frac{N_\tau^{\text{exp}}}{\varepsilon_{\text{TOT}} C_\tau F_\tau(n)}. \qquad (14)$$

Here ε_{TOT} is the product of all experimental efficiencies of the tau analysis

$$\varepsilon_{\text{TOT}} = \varepsilon_{\text{FS}} \varepsilon_{\text{trig}} \varepsilon_{\text{loc}} \varepsilon_\tau. \qquad (15)$$

The efficiencies in Eq. (15) are as follows: filtering and scanning (0.85 ± 0.06), trigger with live time (0.79 ± 0.02), location in emulsion (0.64 ± 0.04), and secondary vertex finding (0.46 ± 0.02), yielding $\varepsilon_{\text{TOT}} = 0.20 \pm 0.02$.

The functional form of $F_\tau(n)$ can be parametrized as

$$F_\tau(n) = 51.6 n^{-1.52}. \qquad (16)$$

This form fits the Monte Carlo calculations to within 10% for $n \geq 4$. Additional details are given in the Appendix.

TABLE VII. Quantities used in the analysis, defined by Eqs. (12) and (13). The values for F_ℓ were estimated using PYTHIA.

Type	$C_\ell \times 10^{40}$ cm^{-2}	F_ℓ GeV
ν_e	1.64 ± 0.38	$4.62^{+1.41}_{-0.94}$
ν_μ	1.55 ± 0.36	$4.33^{+1.32}_{-0.88}$
ν_τ	0.289 ± 0.085	$3.30^{+0.69}_{-0.52}$

TABLE VIII.   The charm hadroproduction cross section results used in the cross section ratios given in Table IX. The D^0 cross section was obtained from the first three results, pN reactions at high energy. The ratio of $D^\pm$ to D^0 was obtained from the first four results (all pN reactions). The ratio of D_s to D^0 was obtained using the last four results. The resulting cross sections are listed in Table VI.

Ref.	Beam type/energy (GeV)	$\sigma(D^\pm)$ μb/nucl	$\sigma(D^0)$ μb/nucl	$\sigma(D_s)$ μb/nucl
[13]	p/800	$37 \pm 9 \pm 12$	$43 \pm 3 \pm 14$	$\cdots$
[14]	p/800	$26 \pm 4 \pm 7$	$22 \pm 8 \pm 6$	$\cdots$
[15]	p/920	$29.9 \pm 4.5 \pm 5.7$	$56.3 \pm 8.5 \pm 9.5$	$\cdots$
[16]	$\pi/250$	$3.3 \pm 0.4 \pm 0.4$	$6.0 \pm 1.4 \pm 0.5$	1.5 ± 1.5
[17]	$\pi/230$	$3.2 \pm 0.2 \pm 0.7$	$6.6 \pm 0.3 \pm 1.0$	2.7 ± 0.2
[16]	$\pi/250$	$3.6 \pm 0.2 \pm 0.3$	$8.7 \pm 0.7 \pm 0.6$	2.0 ± 0.5
[16]	K/250	3.0 ± 0.4	7.2 ± 1.1	3.0 ± 0.9
[18]	$\pi/350$	$3.2 \pm 0.1 \pm 0.3$	$7.8 \pm 0.14 \pm 0.5$	1.3 ± 0.4

B. Systematic uncertainties

The cross section results from this experiment depend on knowing the tau-neutrino flux passing through the emulsion target and the total efficiency for identifying a tau-neutrino interaction. We examine the uncertainties for both of these quantities in more detail.

The value of C_ℓ depends on the number of neutrinos produced in the beam dump, so it is sensitive to variations in the total charm hadroproduction cross section, charm branching ratios, and target atomic number effects, which we parametrize by A^α. The estimated uncertainty in C_τ depends almost entirely on D_s production and decay. The relative uncertainties, computed from quantities listed in Tables VIII, IX, and X, were found to be 0.17, 0.23, and 0.17 for cross section, branching ratio, and A dependence, respectively. Added in quadrature, this gives 0.33 for the

TABLE IX.   The weighted average ratio of $D^\pm$ and D_s cross sections to D^0 for results listed in Table VIII.

Avg. $\frac{\sigma(D^\pm)}{\sigma(D^0)}$	Avg. $\frac{\sigma(D_s)}{\sigma(D^0)}$
0.51 ± 0.06	0.20 ± 0.03

TABLE X.   Leptonic branching fractions of charm and tau used in the analysis [19].

$BR(D_s \to \nu_e X)$	0.08 ± 0.055
$BR(D_s \to \nu_\tau X)$	0.064 ± 0.015
$BR(D_s \to \nu_\mu X)$	0.08 ± 0.055
$BR(D^\pm \to \nu_e X)$	0.161 ± 0.004
$BR(D^\pm \to \nu_\mu X)$	0.161 ± 0.004
$BR(D^0 \to \nu_e X)$	0.066 ± 0.002
$BR(D^0 \to \nu_\mu X)$	0.066 ± 0.006
$BR(\Lambda_c \to \Lambda e^+ \nu_e)$	0.021 ± 0.006
$BR(\Lambda_c \to \Lambda \mu^+ \nu_\mu)$	0.020 ± 0.007
$BR(\tau \to \nu_e X)$	0.1784 ± 0.0005
$BR(\tau \to \nu_\mu X)$	0.1736 ± 0.0005

relative uncertainty in C_τ. The relative errors for charm production of ν_e and ν_μ are taken to be the same for both: 0.10 from charm total cross section, 0.16 from branching ratios, and 0.14 from the A dependence. We adopt the convention to add the errors in quadrature where values are derived from several sources and not likely to be correlated. This gives a total relative systematic error of 0.23 for C_e and C_μ.

The functional form of the n-dependent factor, $F_\tau(n)$, is known from Monte Carlo calculations to be accurate to 10% for all n in the validity range. We use this number as the estimate for the systematic uncertainty.

Using the analog of Eq. (14) for $\ell = e$ or μ one can estimate $C_{e,\mu}$ from the number of ν_μ and ν_e CC interactions in the data ($N_e^{\exp} = 99$, $N_\mu^{\exp} = 137$), given the values of F_ℓ in Table VII, the total efficiencies [$\varepsilon_{TOT}(e) = 0.27$, $\varepsilon_{TOT}(\mu) = 0.33$] and the neutrino cross sections [19]. This provides a systematic check on C_ℓ. The values so derived are $C_e = 1.51 \times 10^{40}$ cm^{-2} and $C_\mu = 1.92 \times 10^{40}$ cm^{-2} (prompt muons only). These are compared with 1.64×10^{40} and 1.55×10^{40}, respectively, from Table VII. This gives an indication that the systematic uncertainty in the charm cross sections, with the charm particle decaying to a ν_e or ν_μ, is reasonably estimated by the value (0.23) given above.

C. Results

The energy-independent part of the ν_τ-nucleon CC cross section was computed using the numbers from Tables V and VII inserted into Eq. (14), with the parametrized form for $F_\tau(n)$:

$$\sigma^{const}(\nu_\tau) = 7.5(0.335 n^{1.52}) \times 10^{-40} \text{ cm}^2 \text{ GeV}^{-1}. \quad (17)$$

The relative statistical error is 0.33 and the relative systematic error is also 0.33. The best estimate for the number of observed ν_τ interactions, 7.5, is shown explicitly. The valid range for the parameter is $n \geq 4$.

Using the PYTHIA-derived value of $n = 6.1$, we give an estimate of the ν_τ CC cross section as
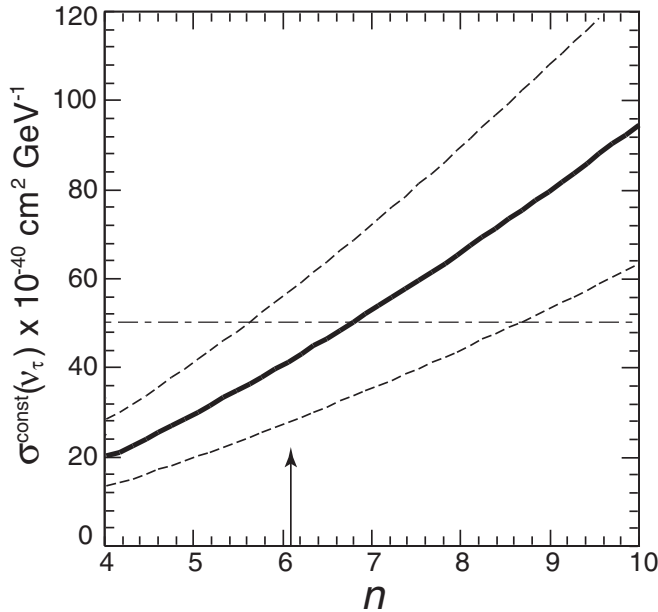
FIG. 16. The energy-independent ν_τ CC cross section as a function of the parameter n in Eq. (7) is represented as the thick solid curve. The 1-σ statistical error is shown by the dashed curves and the average of the standard model ν and $\bar{\nu}$ cross sections is shown by the dot-dashed horizontal line. The arrow shows the expected value of n based on PYTHIA calculations.

$$\sigma^{\text{const}}(\nu_\tau) = (0.39 \pm 0.13 \pm 0.13) \times 10^{-38} \text{ cm}^2 \text{ GeV}^{-1}.$$
(18)

The first error is statistical, the second one systematic. For comparison, assuming lepton universality and an equal number of ν and $\bar{\nu}$, the average energy-independent cross section in the standard model is 0.50×10^{-38} cm^2 GeV^{-1} [19]. The parameter-dependent cross section result is shown graphically in Fig. 16.

Lack of knowledge of the charge of the τ lepton implies that the result, Eqs. (17) and (18), represents an average of ν_τ and $\bar{\nu}_\tau$ cross sections. As discussed in Sec. IX B, the flux of neutrinos in the DONuT beam is approximately equal to the flux of antineutrinos, which has been assumed for the results given above. The actual value of the ratio of ν_μ and $\bar{\nu}_\mu$ fluxes in the DONuT beam was measured to be 1.05 ± 0.13.

XI. CONCLUSIONS

We have analyzed 578 neutrino interactions located in the emulsion target used in the DONuT experiment at Fermilab. Nine ν_τ interactions were observed with an estimated background of 1.5 events. This result was obtained using a multivariate analysis that included correlations between the parameters used in this procedure. The located neutrino events include 120 events identified as ν_e interactions and 225 events identified as ν_μ interactions, consistent with expectations.

In addition, we have obtained a parametrization for the charged-current ν_τ cross section that depends on the longitudinal part of D$_s$ production in 800 GeV pN interactions. At a future date, when this dependence is measured, one can reevaluate the ν_τ cross section, with the result ultimately limited by the relative statistical error.

APPENDIX: CHARM AND TAU PRODUCTION IN 800-GEV PROTON-NUCLEON INTERACTIONS

The majority of the neutrino flux at the DONuT emulsion target originated in charm decays from interactions of 800 GeV protons in the tungsten alloy beam dump. This flux was estimated from results of hadronic charm production in fixed-target experiments. Results from three experiments were used in the following way. First, we fixed the absolute rate of charm production in an 800 GeV proton nucleon using inclusively produced D^0 cross sections from Refs. [13–15,20]. The value of the D^0 cross section from [15] was scaled from 920 to 800 GeV, a factor of 0.84, using PYTHIA [11] with CTEQ6L structure functions before averaging [20]. The weighted mean using the first three entries in Table VIII for D^0 (scaled to 800 GeV) is 41.3 ± 2.6 ± 7.0 μb per nucleon, where the largest relative systematic error of the three is assigned.

We then made the assumption that the ratio of cross sections for producing D$^\pm$ and D$_s$ to that of D^0 production from the same experiment is independent of energy and beam particle. The product of the weighted average of these ratios and the 800 GeV D^0 cross section gives our estimate for the inclusive production cross sections for D$^\pm$ and D$_s$. Table VIII lists the experimental results used in this analysis. Table IX gives the values for the ratios used.

The simulated charm particles produced in the beam dump were forced to decay semileptonically or leptonically with the branching fractions listed in Table X. The charm was produced in a Monte Carlo simulation with a c.m. distribution given by Eq. (7). The value of b was set to 0.8 ± 0.1 [13,14] for the production of all charm mesons. This result from experiments can be compared to the value of b obtained using PYTHIA for D^0, D$^+$ and D$_s$ production of 1.0, 1.0, and 1.1, respectively. The longitudinal dependence, controlled by n, is a function of beam particle, beam energy, and charm species. There are no published data
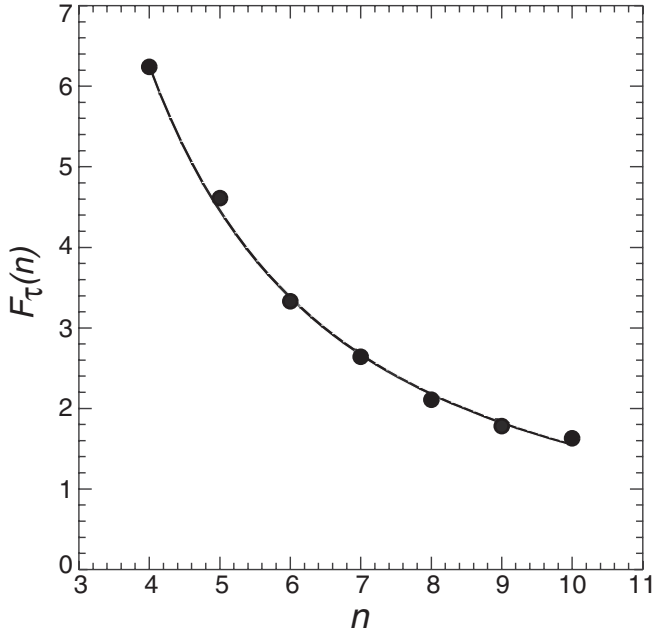
FIG. 17. The computed values of the n-dependent cross section factor, $F_\tau(n)$, for values of n. The functional fit, shown by the line, is given as $F_\tau(n) = 51.6n^{-1.52}$. The points are within 10% for $n \geq 4$.
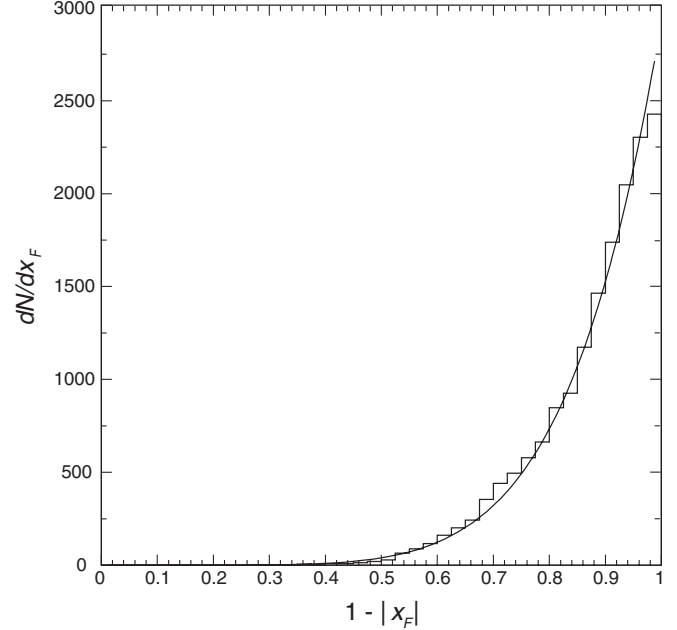

FIG. 18. The $(1 - |x_F|)$ distribution generated from PYTHIA for D_s production in 800 GeV proton-nucleon interactions is shown by the histogram. The fit of this data to a power law is shown as the curve. The fit gives n in Eq. (7) of 6.1 ± 0.1.

giving n for D_s, thus we can only compute the ν_τ flux in the emulsion target as a function of n. This function was computed from the Monte Carlo method by varying the input value of n from 4 to 10. The resulting Monte Carlo computation of $F_\tau(n)$ for discrete values of n is shown in Fig. 17. For values of n less than 4, the function F increases rapidly, becoming very sensitive to geometrical acceptance, and we place a lower limit on the valid range of n. For large n the production of D_s becomes increasingly central and F varies relatively little, and we are confident in the computation. For estimating a particular value for n, we used PYTHIA (version 6.129) [11] to generate D^0, $D^\pm$ and D_s from protons and neutrons. Production in the tungsten beam dump was estimated by weighting with the neutron (60%) and proton (40%) fraction of this nucleus. This yielded values for n of 6.0, 5.7, and 6.1 for D^0, $D^\pm$ and D_s, respectively. These values were input for the DONuT Monte Carlo method to compute the F_ℓ listed in Table VII. The fit to the D_s PYTHIA output is shown in Fig. 18. For comparison, data from two experiments, which did not distinguish charm species, give "average" values of n as 8.6 ± 0.2 [14] and 6.9 ± 1.9 [13].

The simulation of charm production, described above, is appropriate for 800 GeV pN interactions. Charm particles were also produced in hadronic cascade showers in the beam dump, which we call secondary charm production. This secondary production was modeled by GEANT in specific stand-alone calculations. The number of neutrino interactions from secondary charm decays relative to the total was estimated to be 0.075 ± 0.033. This value was applied as a correction to the cross section and was assumed to be independent of flavor. Secondary charm production, from lower energy hadrons, would change the estimated value of n slightly, but we ignore this effect since it accounts for less than 10% of the total observed neutrinos from charm in the beam dump.

Another source of tau neutrinos from the beam dump was B meson semileptonic decay. Although branching fractions are greater than 0.10 [19], the B production cross section is approximately 3 orders of magnitude smaller than for charm [21]. The fraction of ν_τ flux from B mesons is less than 0.02, and was ignored as a source in the Monte Carlo calculations.

[1] M. Perl *et al.*, Phys. Rev. Lett. **35**, 1489 (1975).

[2] C. L. Cowan, F. Reines, F. B. Harrison, H. W. Kruse, and A. D. McGuire, Science **124**, 103 (1956).

[3] G. Danby *et al.*, Phys. Rev. Lett. **9**, 36 (1962).

[4] K. Kodama *et al.* (DONuT Collaboration), Phys. Lett. B **504**, 218 (2001).

[5] B. Lundberg, K. Niwa, and V. Paolone, Annu. Rev. Nucl. Part. Sci. **53**, 199 (2003).

[6] K. Kodama *et al.* (DONuT Collaboration), Nucl. Instrum. Methods Phys. Res., Sect. A **493**, 45 (2002).

[7] K. Kodama *et al.* (DONuT Collaboration), Nucl. Instrum. Methods Phys. Res., Sect. A **516**, 21 (2004).

[8] G. Oleynik *et al.*, IEEE Trans. Nucl. Sci. **41**, 45 (1994).

[9] S. Aoki, Nucl. Instrum. Methods Phys. Res., Sect. A **473**, 192 (2001).

[10] K. Kodama *et al.* (DONuT Collaboration), Nucl. Instrum. Methods Phys. Res., Sect. A **574**, 192 (2007).

[11] T. Sjostrand, Comput. Phys. Commun. **82**, 74 (1994).

[12] J. Sielaff, Ph.D. thesis, University of Minnesota, Minneapolis, MN, 2001; S. A. Rabinowitz *et al.* (CCFR Collaboration), Phys. Rev. Lett. **70**, 134 (1993).

[13] K. Kodama *et al.* (E653 Collaboration), Phys. Lett. B **263**, 573 (1991).

[14] R. Ammar *et al.* (LEBC-MPS Collaboration), Phys. Rev. Lett. **61**, 2185 (1988).

[15] A. Zoccoli *et al.* (HERA-B Collaboration), Eur. Phys. J. C **43**, 179 (2005).

[16] G. A. Alves *et al.* (E769 Collaboration), Phys. Rev. Lett. **77**, 2388 (1996).

[17] S. Barlag *et al.* (ACCMOR Collaboration), Z. Phys. C **49**, 555 (1991).

[18] M. Adamovich *et al.* (WA92 Collaboration), Nucl. Phys. **B495**, 3 (1997).

[19] W. M. Yao *et al.* (Particle Data Group), J. Phys. G **33**, 1 (2006).

[20] C. Lourenço and H. K. Wöhri, Phys. Rep. **433**, 127 (2006).

[21] K. Kodama *et al.* (E653 Collaboration), Phys. Lett. B **303**, 359 (1993).